Journal of Engineering, Science and Technology
ISSN: 2714-2396, Volume 9 Issue 1

FINITE DIFFERENCE SIMULATION OF SWELL PRESSURE-DEPTH AND PRESSURE-TIME VARIATION IN EXPANSIVE SOILS OF THE EASTERN NIGER DELTA AS A GUIDE FOR SUB-STRUCTURAL DEVELOPMENT

O. Festus[1], and E. O. Aigboje[2]*

[1]Department of Mechatronics Engineering], Federal University, Otuoke, Bayelsa State, Nigeria.
[2]Department of Industrial and Production Engineering, Ambrose Alli University, Ekpoma, Nigeria

Corresponding email: aigbojeeddy@gmail.com

Received: 7 April 2026 **Accepted**: Date 23 May 2026 **Published**: 16 June 2026

Abstract. Expansive clays can exert significant swelling pressures (ranging from 50–150 KN/m²) when hydrated, which can uplift or damage structures that are not properly reinforced or designed to resist this pressure. Pipes, ducts, and cables laid within expansive clay soil zones often suffer deformation or rupture due to seasonal ground movement, lateral soil pressure during swelling and void formation due to shrinkage. The above stated adverse effects on engineering structures often leads to high maintenance costs, water loss, and service disruption. In this study, soil swell pressure-depth and soil swell pressure-time data sets were generated from an expansive soil tests conducted in Iwochang-Ibeno, located in the Eastern Niger Delta, region of Bayelsa State, Nigeria. The data were analysed with the respective mathematical governing equations and a soil mesh simulation model is developed to determine the presence of significant soil nodal pressures changes and the times to attain these nodal pressures. A maximum surface soil swell pressure of 6.528 kPa was computed from regression analysis of the Oedometer test data. The value progressively reduced down the soil profile nodes but the pressure at the first node for the zero time increased from 0 kPa to 4.64997 kPa for the 1st node in 26th time at 10 mins time step, while that of the 26th node increased from 0 kPa at the 0th time to 4.53516 kPa in the 26th time. Since these significant pressures exist at the top surface and sub-layers of an expansive soil, it requires that pre-soil treatment be done on such soils before structural development and subsequent scheduled inspection against failure signs for appropriate preventive maintenance.

Keywords: Expansive soil; Swell pressure; Pressure-depth model; Pressure-time model; Soil simulation

1. Introduction

Expansive soils, also known as swell-shrink soils, are a category of clay-rich soils that exhibit substantial changes in volume in response to variations in moisture content. When these soils absorb water, they swell or expand; conversely, when they lose moisture due to evaporation or drainage, they shrink or contract. This cyclic behaviour of swelling and shrinkage can cause significant ground movement, which may be gradual or sudden, depending on the soil type, climatic conditions, and depth of moisture variation. These volume changes can exert tremendous

pressure on any surface and sub-structures, especially shallow foundations, roads, pavements, and lightly loaded buildings, tunnels, sub-ways, buried pipelines, etc. (Onuegbu et al., 2018).
The primary cause of this behaviour is the presence of specific clay minerals, especially montmorillonite, which has a high capacity to absorb and retain water within its crystal structure. Other swelling minerals include smectite and, to a lesser extent, illite. These minerals are characterized by a layered lattice structure that allows water molecules and cations to enter between the layers, increasing the overall thickness and leading to volume expansion (Okugbue and Ezeogenu, 2015 and Okoro et al., 2019).
Globally, expansive soils have been recognized as one of the most problematic soil types in civil and geotechnical engineering. According to Nelson and Miller (1992), expansive soils are responsible for billions of dollars in annual damage to structures worldwide. Unlike other geotechnical problems such as landslides or earthquakes which are sudden and localized, the effects of expansive soils are gradual, widespread, and often go unnoticed until structural damage becomes apparent. Typical manifestations of expansive soil activity include foundation cracks, differential settlement, tilting of structures, heaving of floors, distorted door/window frames and sub-structural deformation like that of pipeline profile deformation due to heaving caused by swell pressure, which in extreme cases, can lead to the total failure of structures.
In the Niger Delta region of Nigeria, the threat of expansive soils is particularly severe due to the region's geological and climatic conditions. The Niger Delta is a low-lying, sedimentary basin with extensive deposits of clay-rich alluvial and marine soils. These soils, formed under tropical humid conditions and influenced by fluctuating groundwater levels and tidal actions, tend to have high moisture retention and plasticity. Additionally, the region experiences significant seasonal variation in rainfall — with extended rainy seasons followed by dry periods — which intensifies the moisture fluctuation in the soil, thereby increasing the magnitude of swelling and shrinkage cycles (Omotosho and Ogboin, 2009).
Urbanization and infrastructural development across the Niger Delta — including major cities such as Port Harcourt, Yenagoa, Warri, and Uyo — have led to the rapid construction of residential buildings, roads, and industrial facilities. Unfortunately, many of these projects were executed without thorough geotechnical investigations, resulting in frequent failures and high maintenance costs. Buildings have developed cracks, pavements have buckled, and roads have deteriorated prematurely, largely due to the underlying expansive clays.

Another aggravating factor is the inadequate drainage systems and improper water management practices in many parts of the region. Prolonged waterlogging during the rainy season, followed by intense drying, creates the perfect conditions for the expansive clay soils to undergo repeated heave and shrinkage cycles. The problem is exacerbated in areas where clay content is particularly high, and where land reclamation projects have disturbed the natural equilibrium of the soil. In this study, we shift the concern on expansive soil from geotechnical analysis to modelling the swell pressure-depth and pressure-time effect of expansive soil to determine sub-soil layers swell pressures and how it progresses with time. This will serve as a guide for surface and sub-surface structural development, and to help predict failure time for any facility in a particular layer from the pressure analysis.

2. Methodology

The method adopted in this study involves the experimental investigation of the presence of expansive clay properties, mathematical analysis of the governing equations of soil pressure depth and pressure time variation and finite difference modelling for a simulated soil nodal pressures at different time step. The data for the simulation process are generated from a soil swell oedometer and Atterberg tests conducted in Iwochang-Ibeno . The Atterberg American Standard Test Method (ASTM 4318) laboratory test for plasticity index to ascertain the presence or otherwise of expansive soil, Oedometer swell pressure test and the mathematical modelling and analysis of soil pressure depth governing equation for a simulated soil nodal pressures were done. A one-dimensional clay soil mesh with nodes listed from top (0 node) to the bottom (N node) along the depth of the soil profile was prepared for simulation and computational analysis.

2.1 Geomorphology and Geology of the Study Area

Iwohcang-Ibeno is an Eastern Niger Delta community in Bayelsa State of Nigeria. It is located on latitude 4.57414°N and longitude 7.94594°E (Fedelis *et al.,* 2018). From Wikipedia (Niger Delta Basin geology), Iwohcang-Ibeno lies within the Niger Delta Basin, one of Africa most significant extensional rift basins formed during the breakup of the South American and African plates. The basin is said to have accumulated up to 9 – 12km of sediment. It is underlain by the sediments of the Benin formation of continental alluvial and flood plain sand and gravel, being the predominant surface geology. This area has the characteristics Niger Delta swamp and buck swamp environments with intertidal zones, mangrove-dominated wetlands transitioning into freshwater swamps or local plains behind levees. A geotechnical study of the area showed a soft, highly compressible Kaolin dominant clay layer extending from ground surface down between 1.0m ad 1.1m in the stream channel and 0.6m to 0.7m in adjacent land areas. This Kaolin layer underlying the surface is overlain by harder clay beneath 4.5 – 5.2m depth, then by loose to medium density sands deeper down, (Fedelis *et al.,* 2018).

A previous soil swell pressure test at approximately1m(0.6m-1.1m) was carried out in Iwochang-Ibeno and a swell potential of 4.8 – 4.9 kPa was recorded with no further record of deeper soil swell pressure. The test showed a result of swell potential of 11.45% - 30.64%, swelling index of 0.44 – 0.57 and swelling pressure of 4.776kPa – 4.890kPa, hence its choice to allow for comparison to ascertain consistency with existing values and validation of the developed nodal pressure model, even though the conducted swell pressure test in this study extend beyond that of the previous report

2.2 Experimental Procedure

The test process in this study is in phases: The Atterberg test for the plasticity index, Oedometer soil swelling pressure test (in time step) and Oedometer soil swell test (varying depth).

2.2.1 Atterberg Test Procedure

The Atterberg limit test procedure according to American Standard Test method (DT4318) was followed in the test process. A 200g sample of clay soil from Iwochang-Ibeno community in Bayelsa State, was filtered or sieved through a 425µm sieve, thereafter, distilled water was added to make a clay paste that has 10% water content and reasonably thick, A triangular groove was cut on the paste after it was loaded into a cup and its surfaced smoothened. The cup is dropped from a height of 1cm (10mm) repeatedly. Other samples are prepared in similar manner with different water content of 15, 20 and 25%. The four specimens are dropped separately in the same manner as the first repeatedly for 25 times and the specimen with the closed groove in the 25th drop represents the water content of the liquid limit (LL) of the clay soil. The water content of four samples excavated from different depths from the same study site and tested with the above procedure are presented in Table 4.1.

In the plasticity limit (PL) test, the ASTM (DT4318) procedure was followed, were 200g of four samples with different water content as before are prepared and rolled into threads in a glass plate. Any of the samples on continues rolling that crumbles at 3m diameter has its moisture content as the soil plastic limit (PL). the results for the plasticity limit are also recorded in Table 4.1, hence the presented results in table 4.1 are the water content of the soil samples at their respective depth.

The soil plasticity index (PI) is the difference between the liquid limit and the plastic limit, which is often reported in percentage. Given that the liquidity limit (LL), the plasticity limit (PL) and the water content of the clay soil sample have been determined from the Atterberg test, the plasticity index (PI) according to Rodrigo (2008) is given as:

$$PI = LL - PL \tag{1}$$

Similarly, the liquidity index is given as

$$LI = \frac{W_c - PL}{PI} \tag{2}$$

where W_c is the soil water content.

2.2.2 Oedometer Swell Pressure Test

The soil swell pressure is the pressure exacted by the soil as it expands due to excess water intake. This pressure varies with depth as it reduces with increasing overburden pressure, varying soil moisture content, density and clay content. Following the Oedometer swell pressure test (ASTM D4546) for undisturbed soil pressure (soil in its original natural state when excavated in a moisture tight condition) four samples of specified sizes were extracted at various depths as presented in Table 4.1. Each sample at a time is trimmed to occupy an Oedometer ring snugly such as to avoid lateral gaps

The sample in the assembling process of the testing is placed between porous stones in the Oedometer cell. The initial height of the soil sample and the dial reading was recorded. A small downward load of 5kPa was applied on the loading arm to ensure proper contact. Water was added to the soil through the Oedometer cell until complete saturation was achieved. To prevent vertical movement of the soil, the vertical dail gauge or the loading yoke was fixed. As pressure develop in the soil through water intake the dial gauge was monitored against vertical movement which implies swelling. On noticing an attempt at movement, more load was added in incremental range of the initial load (5kpa) until no further swelling was noticed at which point, total vertical deformation was achieved. The restraining Weights at this point is the soil swell pressure. This test was repeated for all the other samples at the various depths to record the soil swell pressure at such depths the result is presented in Table 4.2.

For the time-swell pressure test, an undisturbed sample of the same size as the previous ones from the study site is prepared and placed in the Oedometer laid between two porous stones, while the Oedometer cell was properly assemble with the dial gauge in place to record vertical movement (expansion of the soil) and a seating load applied for proper contact.

The sample was flooded with water through the Oedometer cell to achieve saturation. At the instance a vertical movement of the dial gauge was noticed, increment load was added to the loading pan to maintain constant volume, may while the restraining load, the dial reading and the time interval between flooding and this movement is recorded. This process is repeated until zero movement of the dial was achieved at which point the maximum swell pressure had been reached. The test was carried out for the other three samples and results recorded as presented in Table 4.4.

2.3. Analytical Approach

The empirical equations relating soil swell pressure to depth and time as seen from literature are precisely exponential- non- linear(Fredlund and Radhardjo,1993 and Moghaddas and David,2015),hence a regression fitting is done to linearized them for the equations to assume a form that allow for a gradient. Taking the gradient allows for a discretization using the finite difference approach to model the simulation process.

In the simulation design, a clay soil mesh as shown in Fig.1 of N number of nodes was formulated, with the nodes listed from the zero node (top node) to the Nth node at the bottom.

The empirical relationship between soil swell pressure and depth and that of soil swell pressure variability with time is employed in the mathematical modelling of the simulation process. The finite difference method is used in the discretization of the above governing equations. Given that the soil maximum swell pressure (surface pressure) have been estimated from the regression analysis of the soil swell pressure-time test data, the nodal swell pressures and the soil swell nodal pressures at different time steps are computed from the simulated model.

The cross-sectional one-dimensional soil profile swell pressure depth simulation is shown in Figure 1.

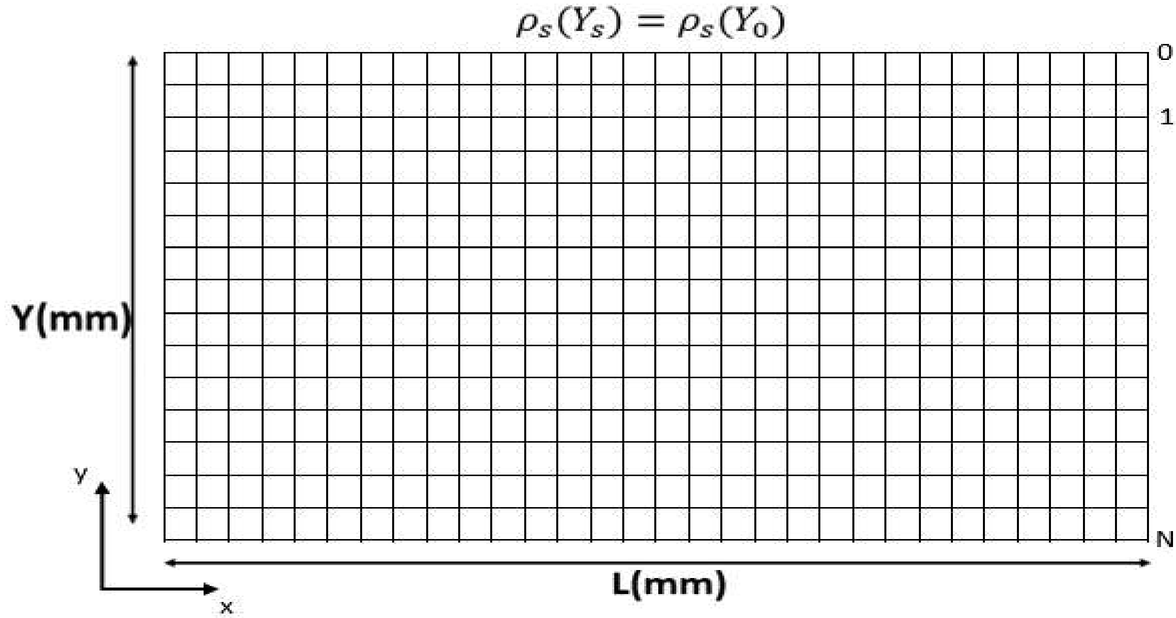

Fig. 1: A computational Model for a Cross-sectional One-Dimensional soil profile swell pressure depth simulation Model.

3.0 Development of the Swell Pressure Depth Model

Given that in an Oedometer swell pressure test, that the swell pressure – depth data for soil sample a, b, c and d for depth layer index j for j = 1, 2, 3, 4 were recorded, then the empirical relationship that exists between the soil swell pressure at the various depths Yj according to Fredlund and Rahardjo (1993) and Chen (1975) is:

$$Ps(Yj) = Ps(Ys)\ e^{(KYj)} \quad (3)$$

where:

j = is the index for the sample's depth, for j = 1, 2, 3, 4.
Ps(Yj) = The soil swell pressure at the jth depth (Yj)
Ps(Ys) = The soil swell pressure at the soil surface
Y = The spatial coordinate of the soil space bounding the samples.
K = Depth decay coefficient determined from regression fitting of the depth pressure records of the test process.
Ys = The depth at the soil surface (depth zero)
The linear form of equation (3) according to Montgomery et al., (2021) and Yanguan (2015) is:

$$\ln Ps(Yj) = \ln Ps(Ys) - KYj \quad (4)$$

Given that the soil mesh of Fig. 1 has N nodes, with i being the index of the nodes such that i = 1, 2,...N, then if we let:

$$\ln Ps(Yi) = Ai \quad (5)$$

$$\ln Ps(Ys) = \theta \quad (6)$$

Substituting equation (5) and (6) into equation (4) gives:

$$Ai = \theta - KYi \quad (7)$$

where Ai = The Natural logarithm of the estimate of the average value of the soil swell pressure for a depth (Yi) of the soil profile; K = The estimate of the slope of the regression line of equation (7); θ = The constant Natural logarithm of the maximum swell pressure which is the estimate of the intercept of the regression line on the swell pressure axis of a plot of swell pressure vs depth.

The values of the constraints θ and k can be estimated according to Ibrahim (2009) for i^{th}

soil layers i = 1, 2..., N:

$$\theta = (\Sigma A + K\Sigma Yi) / N \quad (8)$$

$$K = (\theta\Sigma Yi - \Sigma AiYi) / \Sigma Yi^2 \quad (9)$$

where N = The number of test samples or soil layers. Equation (7) can be transformed into a first order differential form as follows. From the above, the gradient of the straight-line k is given as:

$$K = - dA/dY \quad (10)$$

$$Ai = \theta + Yi(dA/dY) \quad (11)$$

Applying the finite backward difference scheme for the derivative of Y according to Som (2008) gives:

$$dA/dY|Y \approx (Ai - A(i-1)) / \Delta Y \quad (12)$$

Hence equation (11) becomes:

$$Ai = (Yi \times A(i-1) - \theta\Delta Y) / (Yi - \Delta Y), \; for\ i \geq 1, \; Yi \neq \Delta Y \quad (13)$$

where ΔY = Spatial step; Ai = The natural logarithm of the swell pressure at the i^{th} node (current node); A(i−1) = The natural logarithm at the $(i-1)^{th}$ or previous node.

The value of the total number of nodes (N) in the soil mesh for the simulation is given according to Som (2008) and Festus (2025) as:

$$N = Y / \Delta Y + 1 \quad (14)$$

Assuming A_0 is the initial condition given and is equal to θ, then to avoid the error introduced to the recurrent equation (11) in evaluating the initial value of Ai supposing Y = ΔY, the value of A_0 should be determined from equation (7) given that the value of k and θ have been estimated from the regression analysis. Equation (13) can be rearranged to give the matrix form:

$$(\psi i)Ai + (\varphi i)A(i-1) = -\theta \quad (15)$$

where ψi = (Yi/ΔY − 1) and φi = −Yi/ΔY. The above yields a lower bidiagonal matrix for i = 1, 2, ..., N. The initial and top soil boundary condition for the simulation process is:

$$A(Y_0) = A(Ys) \text{ or } A_0 = As = \theta \quad (15a)$$

where As = The natural logarithm of the swell pressure at the top soil layer.

3.1 Development of the Nodal Swell Pressure – Time Model

The nodal soil swell pressure-time test generated the values of the corresponding sample maximum swell pressure at time t. According to Fredlund and Radardjo (1993), the empirical relationship between time and pressure is given as:

$$Ps(t) = (Ps)max\ (1 - e^{-mt}) \quad (16)$$

where Ps(t) = The soil swell pressure at time t; (Ps)max = The maximum surface soil swell pressure; t = Time to attain P(t); m = A decay constant. The linear form of equation (14) by the regression fitting according to Montgomery et al., (2021) and Festus (2024) is:

$$\ln(1 - Ps(t)/(Ps)max) = -mt \quad (17)$$

Setting G(t) = ln(1 − Ps(t)/(Ps)max), then G(t) = −mt. Applying regression modelling gives the m parameter as:

$$m = -\Sigma G(t) / \Sigma t \quad (18)$$

Given a time step n with step size Δt, the finite backward difference scheme applied gives the recurrent relationship:

$$G^n(t) = G^{n-1}(t) - m\Delta t, \quad n = 1, ..., N \quad (19)$$

For the computational model with N nodes, equation (16) transforms for the ith node at the nth time step as:

$$P_{si}^n(t) = Ps(Yi)(1 - e^{G_i^n(t)}) \quad (20)$$

Similarly, from equation (16), the time required to attain pressure P_{si}^n is:

$$t_i = -(1/m) \times \ln(1 - P_{si}^n(t) / Ps(Yi)) \quad (21)$$

4. Results and Discussion

The results of the conducted tests, the calculations based on the results and the subsequent discussions are presented below.

4.1 Results and Analysis of the Atterberg Test

Table 4.1: Oedometer Swell pressure test results for Four clay samples from Iwochang-Ibeno, Eastern Niger Delta, Bayelsa State

Soil Sample	Depth (m)	Soil Distribution	Moisture Content (%)	Plasticity Limit (%)	Liquid Limit LL (%)	Swell Pressure (kPa)
A	0 – 1.5	Soft silty clay	40.0	27.0	53.0	5.20
B	1.5 – 3	Soft silty clay / Organic clay	46.0	20.0	50.0	7.70
C	3 – 4.5	Organic + Clay	49.0	21.0	47.0	8.00
D	4.5 – 6	Firm clayey silts	41.0	22.0	44.0	5.30

Given the entries of table 4.1, the plasticity index for the four samples (a, b, c, d) are evaluated using equation (1) as follows

Recall equation (1), PI = LL – PL
For sample a, LL = 53% and PL = 27%
→ PI = 53 – 27 = 26% (W_c)
Since the water content (W_c) = 40% from equation (2) the liquidity index (LI) is given as:
$LI = \frac{W_c - PL}{PI} = \frac{40-27}{26} = 0.5\%$
For sample b, LL = 50%, PL = 20% W_c = 46%
PI = 50 – 20 = 30% and
$LI = \frac{46-20}{30} = 0.87\%$
For sample c, LL = 47, PL = 21 and W_c= 49
PI = 47 – 21 = 26%
$LI = \frac{49-21}{26} = \frac{28}{26} = 1.1\%$
For sample d, LL = 44, PL = 22 and W_c= 41
PI = 44 – 22 = 22%
$LI = \frac{41-22}{22} = 0.186\%$

4.2 Analysis of the Soil Swell Pressure Depth Test Results

From the entries in Table 4.1, for the swell pressure at various depths Ps(Yi), we have: *A(1.5) = 5.20 kPa = 5200 Pa, ln 5200 = 8.56,*the conversion of the swell pressures from kPa to Pa is necessary to allow for the natural logarithm calculation that requires SI base unit like Pa to maintain dimensional consistency.

A(3) = 7.7 kPa = 7700 Pa, ln 7700 = 8.95

A(4.5) = 8.0 kPa = 8000 Pa, ln 8000 = 8.99

A(6) = 5.3 kPa = 5300 Pa, ln 5300 = 8.58

Table 4.2: Swell Pressure–Depth Regression Data

Data Point j	A(Yj)	Yj (m)	A(yi)Yj	Yj^2
A	8.56	1.5	12.84	2.25
B	8.95	3	26.85	9.00
C	8.99	4.5	40.46	20.25
D	8.58	6	51.00	36.00
Sum	35.08	15	131.15	67.5

From equation (8), θ is given as: $\theta = (\Sigma A + K\Sigma Y) / j = (35 + 15k) / 4$
From equation (9): $270K = 525 + 225K - 524.6$; $45K = 0.4$; $K = 0.4/45 = 0.009$
Hence $\theta = (35 + 15(0.009)) / 4 = 35.135 / 4 = 8.784$
Since $\ln Ps(Y_0) = \theta$, then $Ps(Y_0) = e^\theta = e^{8.784} = 6.528$ kPa. Hence the clay soil surface maximum swell pressure is 6.528 kPa.
Given the estimated values of k and $Ps(Y_0)$, equation (3) for the i^{th} node of the soil mesh for the simulation becomes:

$$Ps(Yi) = 6528 \times e^{-0w009yi}$$

Given that Yi = 0.08 m and ΔYi = 0.08 m, A_0 is determined from Eqn. (7). Recall Eqn. (3): given Ps(Ys) = 6528 Pa, Y = 0.08 m and K = 0.009, then $Ps(0.08) = 6528 \times e^{-0w00072} = 6528 \times 0.99928 = 6523.3$ Pa = 6.53 kPa (the soil mesh second node swell pressure: i = 1). Hence $A_1 = \ln 6523.3 = 8.783$. Similarly, $A_2 = 8.782$. Since the clay profile for the simulation starts from the zero (0) node, the twenty-six node natural logarithms of the maximum swell pressures are generated and the results shown in Table 4.3.

Table 4.3: Natural Logarithms of The Maximum Nodal Soil Swell Pressures for The Soil Profile

Node i	**Ai**
0	8.784
1	8.783
2	8.782
3	8.781
4	8.78
5	8.779
6	8.778
7	8.777
8	8.776
9	8.775
10	8.774
11	8.773
12	8.772
13	8.771

14	8.77
15	8.769
16	8.768
17	8.767
18	8.766
19	8.765
20	8.764
21	8.763
22	8.762
23	8.761
24	8.76
25	8.759
26	8.758

4.3 Results of the Time–Soil Swell Pressure Test

The times to attain various values of pressures for the four soil samples given the maximum swell pressure are recorded in Table 4.4.

Table 4.4: Time swell pressure test results for the four-soil samples

Test Sample	Time (s) t	Max Swell Pressure (kPa)	Load Applied at Time t (kPa)	Dial Reading (mm)
A	4,680	5.20	4	0.020
B	8,928	7.70	6.4	0.050
C	21,600	8.00	7.3	0.070
D	54,000	6.50	5.0	0.090

From the entries of Table 4.4, the respective natural logarithm of the pressures at time (t) are: $Ps(t)a = 4$ kPa; $Ps(t)b = 6.4$ kPa; $Ps(t)c = 7.3$ kPa; $Ps(t)d = 5.0$ kPa.

The G(t) values computed are: $G(t)a = \ln(1 - 4000/5200) = -1.466$; $G(t)b = \ln(1 - 6400/7700) = -1.780$; $G(t)c = \ln(1 - 7300/8000) = -2.436$; $G(t)d = \ln(1 - 5000/6500) = -1.466$.

Table 4.5: The Swell Pressure–Time Regression Data

Sample	G(t)	Time t (s)
A	-1.466	4,680
B	-1.780	8,928
C	-2.436	21,600
D	-1.466	54,000
Σ =	-7.148 /	89,208

From Eqn. (18): m = −(−7.148) / 89208 = 0.000080127 ≈ 0.00008

Given that m = 0.00008, $G_i^0(t) = 0$ (initial condition), Δt = 10 mins = 600 s, subsequent values for $P_{si}^n(t)$ and $G_{23}^n(t)$ are reported in Tables 4.6 and 4.7 respectively from Python code executed. Selected key results are: for i = 0 and n = 1: $G_0^1 = −0.048$; for node i = 20 and n = 1: $Ps(Y_{20})$ = e^8.764 = 6399.65 Pa; $Ps_{20}(600)$ = 6399.65(1 − e^$^{−0w00008}$ × 600) = 299.93 Pa. For node i = 23: $Ps(Y_{23})$ = e^8.761 = 6380.49 Pa; $Ps_{23}^1(600)$ = 299.03 Pa.

Table 4.6; The Nodal Soil Swell Pressures for Different Time Steps.

	i=1	i=2	i=3	i=4	i=5	i=6	i=7
n=1	305.681	305.375	305.07	304.765	304.461	304.156	303.852
n=2	597.036	596.439	595.843	595.247	594.652	594.058	593.464
n=3	874.736	873.861	872.988	872.116	871.244	870.373	869.503
n=4	1139.42	1138.28	1137.14	1136.01	1134.87	1133.74	1132.61
n=5	1391.7	1390.31	1388.92	1387.53	1386.15	1384.76	1383.38
n=6	1632.16	1630.53	1628.9	1627.27	1625.64	1624.02	1622.4
n=7	1861.35	1859.49	1857.63	1855.77	1853.92	1852.06	1850.21
n=8	2079.79	2077.71	2075.64	2073.56	2071.49	2069.42	2067.35
n=9	2288	2285.72	2283.43	2281.15	2278.87	2276.59	2274.32
n=10	2486.45	2483.97	2481.49	2479	2476.53	2474.05	2471.58
n=11	2675.6	2672.93	2670.26	2667.59	2664.92	2662.26	2659.6
n=12	2855.89	2853.03	2850.18	2847.33	2844.49	2841.64	2838.8
n=13	3027.72	3024.7	3021.68	3018.66	3015.64	3012.62	3009.61
n=14	3191.51	3188.32	3185.13	3181.95	3178.77	3175.59	3172.42
n=15	3347.61	3344.27	3340.93	3337.59	3334.25	3330.92	3327.59
n=16	3496.41	3492.91	3489.42	3485.93	3482.45	3478.97	3475.49
n=17	3638.22	3634.59	3630.95	3627.32	3623.7	3620.08	3616.46
n=18	3773.39	3769.62	3765.86	3762.09	3758.33	3754.57	3750.82
n=19	3902.23	3898.33	3894.43	3890.54	3886.65	3882.77	3878.89
n=20	4025.03	4021.01	4016.99	4012.97	4008.96	4004.95	4000.95
n=21	4142.07	4137.93	4133.8	4129.66	4125.54	4121.41	4117.29
n=22	4253.63	4249.38	4245.13	4240.89	4236.65	4232.41	4228.18
n=23	4359.96	4355.6	4351.25	4346.9	4342.55	4338.21	4333.88
n=24	4461.3	4456.85	4452.39	4447.94	4443.5	4439.05	4434.62
n=25	4557.9	4553.35	4548.79	4544.25	4539.71	4535.17	4530.64
n=26	4649.97	4645.32	4640.68	4636.04	4631.41	4626.78	4622.15

i=8	i=9	i=10	i=11	i=12	i=13	i=14	i=15
303.549	303.245	302.942	302.639	302.337	302.035	301.733	301.431
592.871	592.278	591.686	591.095	590.504	589.914	589.324	588.735
868.634	867.766	866.898	866.032	865.166	864.302	863.438	862.575
1131.47	1130.34	1129.21	1128.08	1126.96	1125.83	1124.7	1123.58
1381.99	1380.61	1379.23	1377.85	1376.48	1375.1	1373.73	1372.35
1620.77	1619.15	1617.54	1615.92	1614.3	1612.69	1611.08	1609.47

1848.36	1846.52	1844.67	1842.83	1840.98	1839.14	1837.31	1835.47
2065.29	2063.22	2061.16	2059.1	2057.04	2054.98	2052.93	2050.88
2272.04	2269.77	2267.5	2265.24	2262.97	2260.71	2258.45	2256.19
2469.11	2466.64	2464.18	2461.71	2459.25	2456.79	2454.34	2451.89
2656.94	2654.28	2651.63	2648.98	2646.33	2643.69	2641.05	2638.41
2835.97	2833.13	2830.3	2827.47	2824.65	2821.82	2819	2816.18
3006.6	3003.6	3000.6	2997.6	2994.6	2991.61	2988.62	2985.63
3169.25	3166.08	3162.91	3159.75	3156.59	3153.44	3150.29	3147.14
3324.26	3320.94	3317.62	3314.31	3310.99	3307.68	3304.38	3301.07
3472.02	3468.55	3465.08	3461.62	3458.16	3454.7	3451.25	3447.8
3612.84	3609.23	3605.63	3602.02	3598.42	3594.83	3591.23	3587.64
3747.07	3743.33	3739.59	3735.85	3732.11	3728.38	3724.66	3720.93
3875.01	3871.14	3867.27	3863.4	3859.54	3855.68	3851.83	3847.98
3996.95	3992.96	3988.97	3984.98	3981	3977.02	3973.04	3969.07
4113.18	4109.07	4104.96	4100.86	4096.76	4092.66	4088.57	4084.49
4223.96	4219.74	4215.52	4211.31	4207.1	4202.89	4198.69	4194.49
4329.55	4325.22	4320.9	4316.58	4312.26	4307.95	4303.65	4299.34
4430.18	4425.76	4421.33	4416.91	4412.5	4408.09	4403.68	4399.28
4526.11	4521.58	4517.06	4512.55	4508.04	4503.53	4499.03	4494.54
4617.53	4612.92	4608.31	4603.7	4599.1	4594.5	4589.91	4585.32

i=16	i=17	i=18	i=19	i=20	i=21	i=22	i=23
301.13	300.829	300.528	300.228	299.928	299.628	299.329	299.029
588.147	587.559	586.972	586.385	585.799	585.214	584.629	584.044
861.713	860.851	859.991	859.131	858.273	857.415	856.558	855.702
1122.46	1121.34	1120.21	1119.1	1117.98	1116.86	1115.74	1114.63
1370.98	1369.61	1368.24	1366.88	1365.51	1364.14	1362.78	1361.42
1607.86	1606.25	1604.65	1603.04	1601.44	1599.84	1598.24	1596.64
1833.63	1831.8	1829.97	1828.14	1826.31	1824.49	1822.67	1820.84
2048.83	2046.78	2044.74	2042.69	2040.65	2038.61	2036.57	2034.54
2253.94	2251.69	2249.43	2247.19	2244.94	2242.7	2240.46	2238.22
2449.43	2446.99	2444.54	2442.1	2439.66	2437.22	2434.78	2432.35
2635.77	2633.13	2630.5	2627.87	2625.25	2622.62	2620	2617.38
2813.37	2810.56	2807.75	2804.94	2802.14	2799.34	2796.54	2793.75
2982.65	2979.67	2976.69	2973.71	2970.74	2967.77	2964.81	2961.84
3143.99	3140.85	3137.71	3134.57	3131.44	3128.31	3125.18	3122.06
3297.78	3294.48	3291.19	3287.9	3284.61	3281.33	3278.05	3274.77
3444.35	3440.91	3437.47	3434.03	3430.6	3427.17	3423.75	3420.32
3584.06	3580.47	3576.9	3573.32	3569.75	3566.18	3562.62	3559.06
3717.22	3713.5	3709.79	3706.08	3702.38	3698.68	3694.98	3691.29
3844.13	3840.29	3836.45	3832.62	3828.79	3824.96	3821.14	3817.32
3965.1	3961.14	3957.18	3953.23	3949.28	3945.33	3941.38	3937.45
4080.4	4076.33	4072.25	4068.18	4064.12	4060.05	4056	4051.94

4190.3	4186.11	4181.93	4177.75	4173.57	4169.4	4165.23	4161.07
4295.05	4290.75	4286.47	4282.18	4277.9	4273.63	4269.35	4265.09
4394.88	4390.49	4386.1	4381.72	4377.34	4372.97	4368.59	4364.23
4490.04	4485.56	4481.07	4476.59	4472.12	4467.65	4463.18	4458.72
4580.74	4576.16	4571.59	4567.02	4562.46	4557.9	4553.34	4548.79

Table 4.7: $G_{23}^n(t)$ (The Natural Logarithm of the Ratio of the Twenty -third Nodal Pressure to the Maximum Soil Surface Pressure Minus One

Node	n=1	n=2	n=3	n=4	n=5	n=6	n=7	n=8
i=23	-0.048	-0.096	-0.144	-0.192	-0.24	-0.288	-0.336	-0.384

n=9	n=10	n=11	n=12	n=13	n=14	n=15	n=16	n=17
-0.432	-0.48	-0.528	-0.576	-0.624	-0.672	-0.72	-0.768	-0.816

n=18	n=19	n=20	n=21	n=22	n=23	n=24	n=25	n=26
-0.864	-0.912	-0.96	-1.008	-1.056	-1.104	-1.152	-1.2	-1.248

4.4 Discussion

The clay soil samples were excavated from Iwochang-Ibeno area of Bayelsa state, being about the only area where recorded soil swell pressure time test has been conducted in Nigeria, though at shallow depth (0.6 - 1.10m). Hence its choice to establish consistency or otherwise in comparing the published results (4.776kPa - 4. 890KPa) with that of this study, which according to the test results of table 4.1 gave a swell pressure of 5.20KPa for a depth of 0 – 1.5m. This result at the shallow depth is consistent with previous one, which gives reasonable confidence level of acceptance for those of the deep layer samples. The Atterberg test results presented in table 4.1 show plasticity index PI fluctuating between 22% and 30% due to the soil varying organic and water content. In the same vein, the liquidity index (LI) varied between 0.5 and 1.1%, hence indicating the presence of low to medium expansive soil by the reports of Avwenagba *et al* (2014). The four clay samples-a, b, c and d excavated from depths, 0-1.5, 1.5-3, 3-4.5 and 4.5-6m respectively, showed high plasticity index (high range of soil water content for which the soil behaves plastically), of 26%, 30%, 26%, and 22%, indicating that the tested soil contains active clay minerals indicating the presence of expansive, coercive and high plastic clay. All the samples with liquidity index (LI) greater than zero and less than 1 except for sample (c) indicate that the tested clay soil excavated at such depths are in plastic state (can be -depth regression equation modeld without cracking or crumbling). Sample c with PI>1 indicate soil that behaves as liquid. The two Atterberg parameters (PI & LI), confirm the presence of expansive soil. The swell pressure formulated from the analysis of the test results shows that the soil swell pressures evaluated and presented in Table 4.3 decreased with the soil profile depth in line with Fredlund and Rahardjo (1993) and Chen (1975). From the entries of Table 4.3, it can be seen that the natural logarithm of the nodal pressure decreased by 0.001 from the zero node to the 26th node. The natural logarithm of the soil surface swell pressure is 8.784 (6.528 kPa). The entries of the soil nodal pressure across the soil mesh in Table 4.6 show that there is an increase with time. The pressure at the first node for the first-time step was 305.681 Pa and progressed to 4.650 kPa at the 26th time step; similarly, that of the 26th node progressed from 298.134 Pa for the first -time step to 4.535 kPa at the 26th time step for a time step of 10 mins.

4.5 Findings

The study found that soil swell pressure increases with time across sub-soil layers even though the pressure is higher at the soil top surface. Hence at some point in time, the soil swell pressure will be enough to significantly counterbalance the applied load of any surface or sub-surface structure, thereby resulting in failure through structural profile deformation from heave stresses or foundational shift.

5. Study Limitations

One of the outstanding limitations of this study is the lack of real-life soil profile pressures for deep soil from Eastern Niger Delta of Nigeria particularly Iwochang-Ibeno. Even though the shallow soil simulation of the developed model is in the same range with those reported in the study of Fidelis *et al. (*2018) which is the most comprehensive report of soil swell pressure test in the study area, lack of deeper soil test results makes comparison of the simulated results impossible and suggests that the results should be applied with caution.

6. Conclusion

Soil swell pressure variation with depth and time has been successfully developed in this study as a guide to potential surface and sub-surface structural developers for informed decision on the right layers of least pressure as sites for such structures and advance failure time information against the backdrop of the nodal pressure after a given time step. This guide serves to complement expansive soil treatments, such as proper drainage, pile foundation and lime treatment, etc. It is particularly instructive in the prediction of the failure time for buried pipeline network and other sub-surface facilities.

References

Onuegbu, O. U., Ogboin, A. S. and Nwoji, C. U. (2018). Characterization of Engineering Properties of Active Soil stabilized with Nanomaterials for Sustainable Infrastructure Delivery. Frontiers in Sustainable Design and Construction, vol. 4.

Okogbue, C. O. and Ezeogenu, N. E. (2015). Stabilization of expansive soils using fly ash and lime. Journal of Civil Engineering and Construction Technology, 6(8), pp. 101–109.

Okoro, L. C., Okeke, O. C. and Opara, A. I. (2019). Evaluation of Treatment of Swelling Behavior of Expansive Soil in Part of Ohafia South-Eastern Nigeria. Advance Journal of Current Research, vol. 6, No. 4.

Omotosho, O. and Ogboin, A. S. (2009). Active Soils of the Niger Delta In Road Pavement Design and Construction. Geotechnical and Geological Engineering, vol. 27, pp. 81–88.

Fidelis, A., Teme, S. C. and Oborie, E. (2018). Geotechnical considerations of the design and construction of foundations in marshy stream channel of Iwochang-Ibeni, Eastern Niger Delta, Nigeria. Journal of Civil, Construction and Environmental Engineering, vol. 3, issue 6.

Fredlund, D. G. and Rahardjo, H. (1993). Soils Mechanics for Unsaturated Soils. John Wiley & Sons, New York.

Moghaddas Tatreshi, S. N. and Norouzi, M. (2015). Effect of Expansive Clay Heave on Burial Pipes. Geotechnical and Geological Engineering, vol. 32(2), pp. 243–253.

Montgomery ,D.C., Peak, E.A and Vim G.G.(2021). Introduction to Linear Regression Analysis (6th Edition),Wiley.
Yanguan C.(2015).The Distance Decay Function of Geographical Gravity Model .Power Law or Exponential Law.arriv:02915[physics.soc.ph]
Som, S. K. (2008). Introduction to Heat Transfer. Prentice-Hall of India, New Delhi.
Festus, O. (2025). Determining the Impact of Maintenance and Salvage Cost's Function Parameters on an Equipment Optimal Replacement Time Computation Under the Economic Life Cycle Strategy: Case Study of a Commuter Bus. World Journal of Innovation and Modern Technology, vol. 9, no. 4, pp. 18–35..
Festus, O. and Mbamabu, E. (2024). Effective Tracking of Hostility Against Humanitarian Aid Workers: A Rescue Time-Mortality Modelling and Rated Security Approach. International Journals of Engineering Science, vol. 11, pp. 103.
Festus Owu and Ernest Mbamabu, E. (2024). Effective Tracking of Hostility Against Humanitarian Aid Workers: A Reserve Time-Mortality Modelling and Rated Security Approach. International Journals of Engineering Science, Vol.11.